THE JOURNAL OF PHYSICAL CHEMISTRY C
A JOURNAL OF THE AMERICAN CHEMICAL SOCIETY

pubs.acs.org/JPCC

Article

Nonclassical Nucleation of Hexagonal Boron Nitride Enables Independent Control of Nucleation and Growth Rate

Dominik Steiner,* Marco Thaler, Thomas Mairegger, Florian Mittendorfer, and Erminald Bertel*

Cite This: *J. Phys. Chem. C* 2023, 127, 11559−11569

Read Online

ACCESS | Metrics & More | Article Recommendations | Supporting Information

ABSTRACT: Growth of high-quality, large-scale hexagonal boron nitride (h-BN) monolayers requires either an extremely low nucleation density or the seamless coalescence of identically oriented nuclei. We report on the nucleation process of h-BN on Pt(110), a substrate on which large single-crystalline domains can be obtained. Nucleation was investigated by scanning tunneling microscopy and UV photoemission. Neither self-collimated growth nor step-induced grain orientation can explain the scarcity or absence of twin domains, which here is caused by an extremely low nucleation density primarily owing to nonclassical nucleation. Key to the unexpected single-domain growth on a template with different symmetry is the instability of the Pt(110) surface layer, which adapts to the h-BN structure at high temperatures in different ways depending on the size of the h-BN islands. The resulting nonclassical nucleation offers additional levers, which allow reconciling low nucleation density with high growth rates, while in classical nucleation, a low nucleation rate is invariably tied to low growth rate.

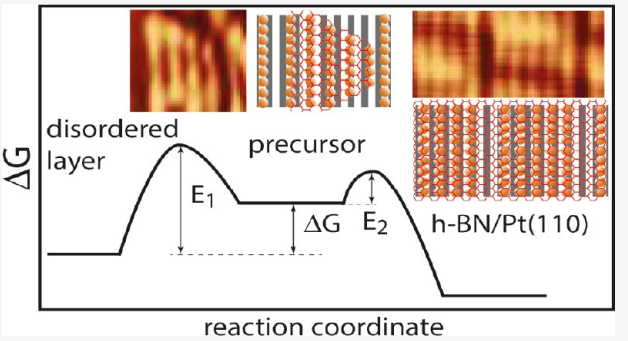

1. INTRODUCTION

Hexagonal boron nitride (h-BN) monolayers are a fascinating two-dimensional (2D) material offering several attractive properties for diverse technological applications. Most prominently, it provides an excellent platform for graphene-based electronics.[1] It is a nearly ideal template for epitaxial graphene growth and, with a band gap of ∼6 eV, serves at the same time as an ultrathin insulating layer. Optical applications exploit its hosting of single-photon emitting defects with excellent spectral properties.[2] Phonon−polaritons in h-BN allow extreme light confinement and promise among other things applications in microinfrared spectroscopy.[3,4] h-BN is also explored with respect to catalysis,[5] membrane technology,[6] tribology,[7] and other areas, where the promise of 2D materials is more and more recognized.[8]

While the growth of monatomic layers of h-BN became almost routine in recent years,[9] important aspects of the growth mechanism are not yet sufficiently understood. Recently, several cases of single-domain growth have been reported, but the mechanisms favoring the formation of large 2D single crystals are under discussion. In particular, it is an open question of how to avoid line defects, such as grain boundaries between differently oriented islands. The Frenken group, for instance, studied h-BN growth on Rh(111) by high-temperature scanning tunneling microscopy (HT-STM) and concluded that the seams between coalescing nuclei do not anneal at high temperatures but persist as fault lines.[10] Accordingly, their recommended recipe for optimal films was to combine a low flux and a high diffusion coefficient (viz. high temperature) in order to suppress the nucleation density as much as possible. This scenario poses two obstacles for industrial application of two-dimensional (2D) h-BN. First, low flux means low growth rates. Second, if the homogeneous nucleation is sufficiently low, heterogeneous nucleation will take over. In this case, the number of defects in the substrate, which serve as heterogeneous nucleation centers, determines the limit for reducing the number of fault lines.

Multiple nucleation, in contrast, requires identical orientation of nuclei for enabling seamless coalescence. For fcc(111) surfaces, Zhao et al.[11] investigated the most stable configurations of triangular nuclei, showing that the preference for B in hcp and N in on-top sites could favor a unique orientation. However, formation energies for mirror nuclei are similar, and very high barriers separate the two energy minima. Thus, it is somewhat surprising if only one minimum is populated after cooling down from the high preparation temperature (>1000 K). Indeed, it is not quite clear which experimental conditions lead to a unique orientation.[12]

Lee et al. obtained seamless film growth on a liquid Au surface.[13] They attributed this surprising result to facile

Received: January 10, 2023
Revised: May 23, 2023
Published: June 12, 2023

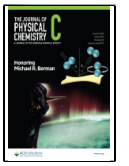

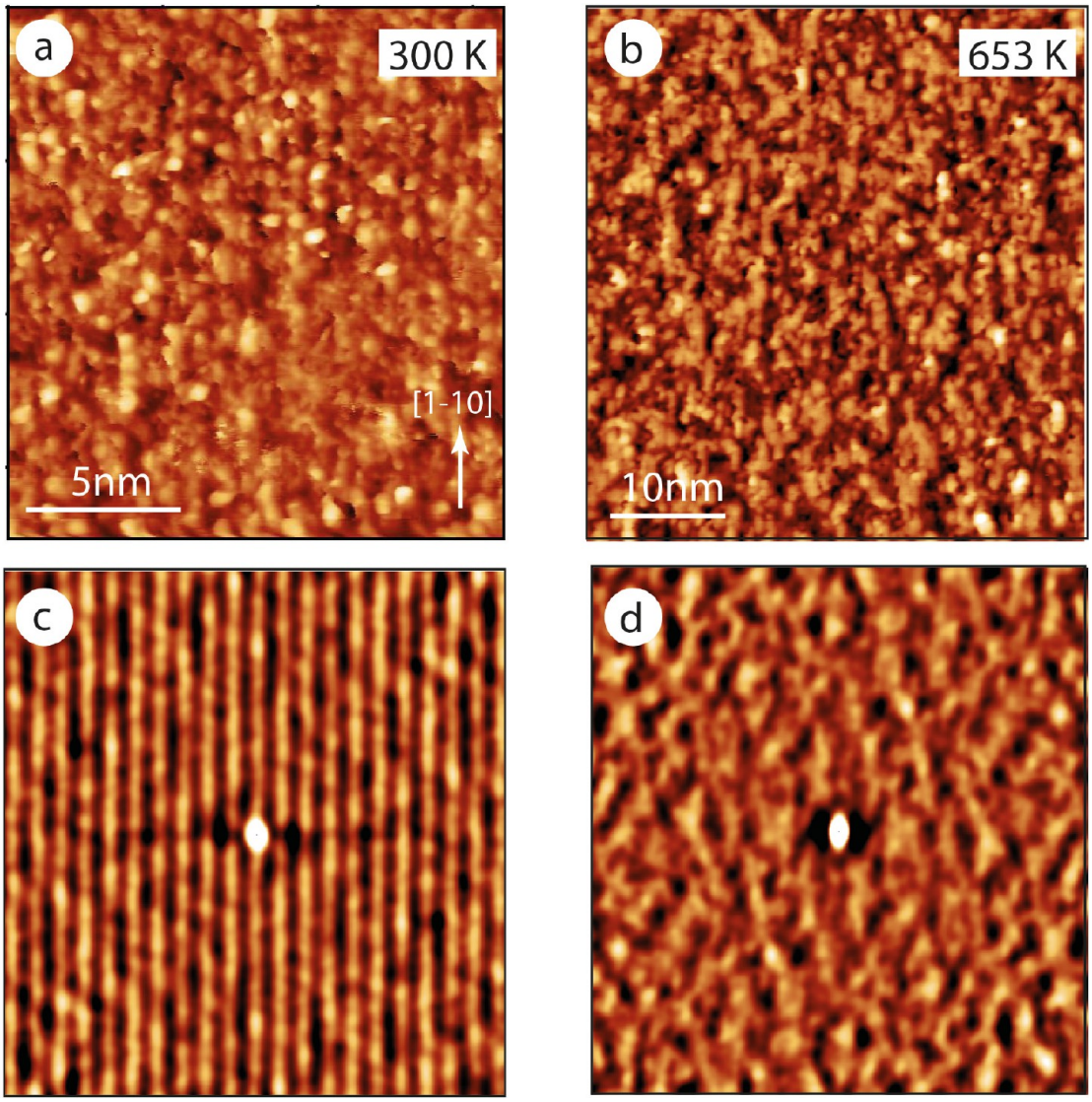

Figure 1. STM images recorded after saturation adsorption of borazine at T = 120 K and subsequent annealing. The STM data were recorded at 300 K. (a) After annealing to 300 K (U_{bias} = 1.0 V, I_t = 700 pA). (b) After annealing to 653 K (U_{bias} = 2.0 V, I_t = 200 pA). (c) 2D autocorrelation of image (a), revealing the (1 × 2) m.r.-row reconstructed Pt(110) surface underneath the disordered adsorbate layer. (d) 2D autocorrelation of image (b), showing the loss of order in the Pt(110) surface.

rotation of the h-BN nuclei on the liquid surface caused by the electrostatic attraction of B and N. Steiner et al. reported extended single-domain h-BN monolayer growth on Pt(110) at temperatures above the roughening transition of Pt(110).[14] Since this implies a high mobility of Pt surface atoms, they rationalized their result in a similar way as Lee et al., i.e., as growth on a quasiliquid layer. Accordingly, optimal single-crystal growth should be more or less independent from the particular surface orientation and generally be achievable above premelting transition temperatures.

Yakobson and co-workers[15] brought forward still another proposal for obtaining single-crystal h-BN monolayers, namely by docking of nuclei at properly oriented steps. They assume nucleation to occur at steps, facilitated by the excess binding energy of zigzag N edges (ZN edges in the terminology of the authors) to the step atoms. Since the steps exhibit kinks, particularly at the high temperatures applied during h-BN growth, geometric matching between step kinks and ZN edge kinks is thought to be a prerequisite for an extended nesting of the h-BN nuclei to the steps. This leads to a unique orientation of the nuclei, a necessary condition for their fusion to uniform large-scale domains. Such a mechanism, for instance, was claimed to be the cause for wafer-scale single-domain growth of h-BN on vicinal Cu(111).[16,17] With respect to Cu(110) and Pt(110), Yakobson and co-workers predicted that <112> steps should provide appropriate docking sites for nucleation and preferential orientation of h-BN nuclei.[15] Thus, vicinal template surfaces offering the required step orientations and breaking the mirror symmetry are recommended for preparation of uniform films. As mentioned above, we found indeed that the single-domain growth occurred at deposition temperatures above the Pt(110) roughening temperature,[14] where the step free energy goes to zero. Note, however, that in this case roughening implies foremost proliferation of <1−10> steps rather than <112> steps. Furthermore, even if thermal fluctuations produce <112> steps, the C_{2v} symmetry of fcc(110) surfaces persists. Accordingly, two h-BN domains are expected with about 10° misorientation relative to each

https://doi.org/10.1021/acs.jpcc.3c00206
J. Phys. Chem. C 2023, 127, 11559−11569

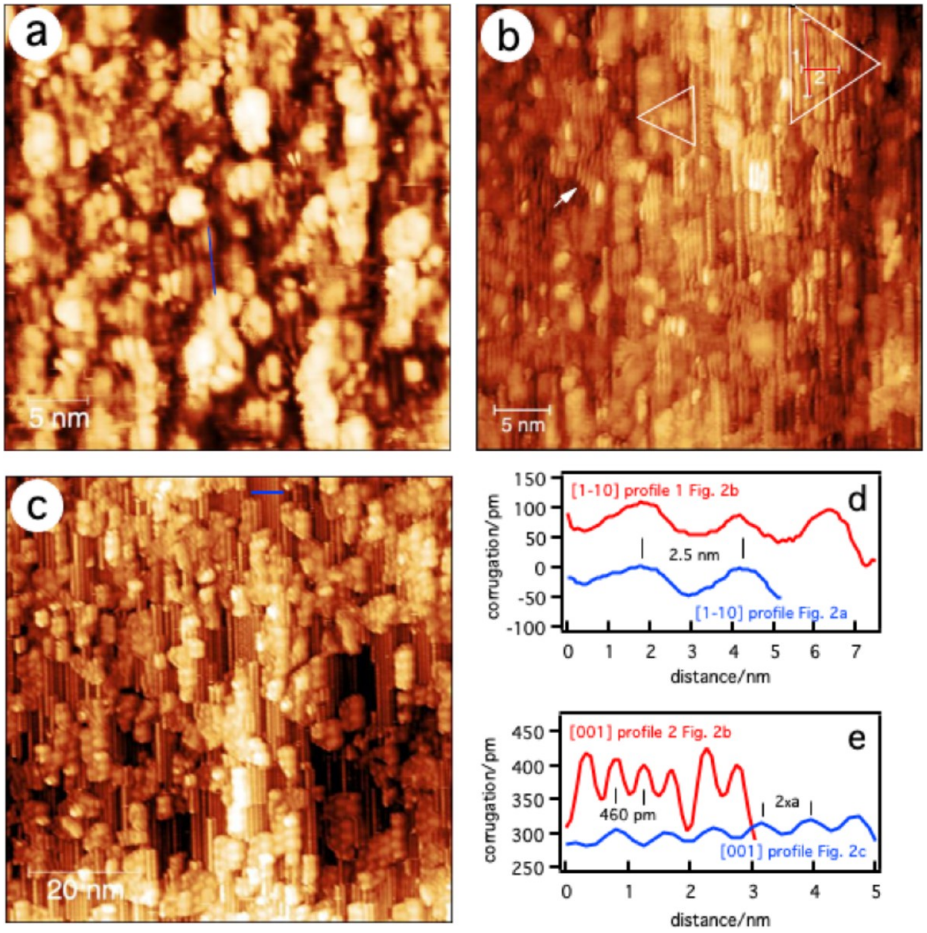

Figure 2. (a) STM image of a borazine layer annealed to 973 K for 3 min (U_{bias} = 0.8 V, I_t = 1.3 nA). (b) Borazine layer heated to 1143 K for 1 min. White triangles mark oppositely oriented h-BN precursor nuclei. The white arrow points to a patch with an oblique orientation of Pt rows (U_{bias} = 0.8 V, I_t = 1.0 nA). (c) Borazine layer heated to 1143 K for an additional 4 min (U_{bias} = 0.7 V, I_t = 1.2 nA). (d) Corrugation measured along the blue profile in Figure 2a and along the red profile 1 in Figure 2b. (e) Corrugation measured along the blue profile in Figure 2c (close to the top) and along the red profile 2 in Figure 2b. The blue profile is taken on a patch of a clean, (1 × 2) m.r. reconstructed Pt surface and serves for calibration (periodicity 2 × a = 784 pm, a being the Pt lattice constant).

other (the <112> steps include an angle of 70°, the h-BN zigzag edges an angle of 60°). We will show below that even an inadvertent symmetry break due to a slight misalignment of the surface orientation cannot explain the present results. Thus, at least for Pt(110), the step-ZN edge nesting has to be eliminated as a possible cause for single-domain growth.

Apart from the question of which of the above mechanisms governs the development of large, 2D single-crystal areas of h-BN on Pt(110), the h-BN nucleation process itself is not yet clear.

We tried to produce h-BN nuclei by reducing the flux during high-temperature exposure to borazine or, alternatively, by reducing the exposure time at high dosing pressure. In both cases, we were able to reduce the coverage, but we always got islands spanning terraces in [001] direction completely from step to step and totally empty terraces. We were not able to prepare terraces with isolated h-BN nuclei. Below a certain threshold value of borazine pressure, no h-BN was nucleated at all.

In order to learn more about the nucleation mechanism, we therefore compared three different preparation protocols: The first one was starting from a saturated borazine monolayer on Pt(110) followed by subsequent heating of the adsorbate layer to successively higher temperatures.[18] For the second one, an h-BN film was deposited at a sample temperature of 970 K, yielding a rough surface with a strongly defective h-BN layer,[14,19] which was then stepwise annealed to higher temperatures as described below. The third one consisted of exposure to borazine vapor at sample temperatures above 1120 K.[14] All three protocols produced different results, showing that the classical nucleation mechanism does not work in the present system. Rather, the data reveal a dynamic participation of the topmost Pt layer in the film formation. Transiently, at high temperatures, a *dynamic* h-BN/Pt double layer is formed, which only in a second step transforms into the (1 × n) missing-row (m.r.) Pt(110) surface supporting a defect-free, single-domain h-BN monolayer. The transformation process yields terrace widths substantially exceeding those of the pristine surface.

2. METHODS

A description of the experimental setup is given in ref 14. In most of the experiments, borazine was dosed from a storage vessel cooled by a Peltier cooling element. Experience showed, however, that degradation of borazine kept at a few mbar in a stainless-steel vessel at room temperature was rather slow. Hence, continuous cooling is not mandatory for such low-pressure storage vessels. The borazine was dosed onto the

https://doi.org/10.1021/acs.jpcc.3c00206
J. Phys. Chem. C 2023, 127, 11559−11569

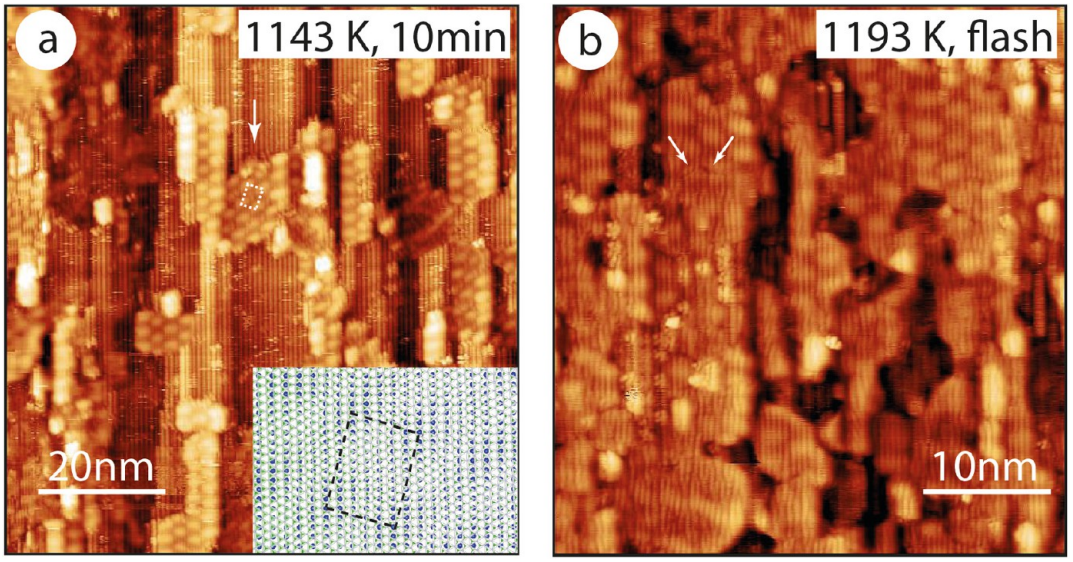

Figure 3. (a) STM image of a saturated borazine layer heated for 10 min to 1143 K (U_{bias} = 1.0 V, I_t = 1.0 nA). The white arrow designates a slightly rotated h-BN flake. Inset: moiré pattern obtained for a slightly counterclockwise rotated h-BN layer so that the B−N zigzag rows deviate by 1.5° from the [1−10] direction. The dashed rectangles delineate the moiré unit cell. (b) Saturated borazine layer flash annealed to 1193 K (U_{bias} = 0.6 V, I_t = 1.4 nA). White arrows point at a grain boundary.

sample through a capillary to keep the background pressure in the preparation chamber during exposure below 10^{-7} mbar. After the annealing procedures, we always used a controlled cooling rate of 1 K/s down to 940 K. LEED intensity measurements were carried out by recording profiles of several moiré induced LEED spots (marked by circles in Figure 4). The intensity was then determined from an average of peak heights. A primary energy E_p = 62 eV was used for all LEED images.

The DFT calculations were performed for a c(10 × 10) superstructure supported on a three layer Pt(110) slab using the Vienna Ab-Initio Simulations package[20,21] and the Perdew−Burke−Ernzerhof (PBE) xc functional[22] with DFT-D3 corrections.[23] Details on the computational setup can be found in ref 14.

3. RESULTS

3.1. Protocol 1: Annealing of Preadsorbed Borazine.

Figure 1a shows an STM image recorded after adsorption of borazine at 120 K and subsequent annealing to room temperature (RT). The surface is obviously completely covered by a disordered overlayer. At 300 K, a substantial amount of borazine is already dehydrogenated, as demonstrated in our recent borazine decomposition study.[18] Nevertheless, the (1 × 2) missing-row reconstruction of the underlying Pt(110) surface is still visible. This is clearly reflected in the 2D autocorrelation image shown as Figure 1c. Basically, the 2D autocorrelation is defined here as

$$F(\vec{r}) = \frac{1}{S}\iint_S z(\vec{x})z(\vec{x}+\vec{r})\mathrm{d}^2x \quad (1)$$

where $z(\vec{x})$ is the (apparent) height coordinate. Features $z(\vec{x}_i)$ that periodically recur at distances $n\vec{r}_0$ add as $nz^2(\vec{x}_i)$ to $F(\vec{r}_0)$. Random features, in contrast, average out to a smooth background. Thus, the autocorrelation acts as a filter emphasizing periodic features. For Figure 1c, we used the discrete implementation of eq 1 in Gwyddion.[24] Although borazine fragments adsorbed via N in an upright configuration desorb recombinatively even below RT, the surface coverage is still close to monolayer saturation at RT, since this species amounts to only a few percent as shown in ref 18. Cracking of B−N rings seems to start at T > 170 K, but the majority of B−N σ bonds survives up to RT. The disordered layer on top of the undisturbed (1 × 2) m.r. Pt(110) surface exhibits an rms roughness of only ∼44 pm (measured along a linear profile; the absolute value is of little significance, but the changes upon different preparations are informative). In the next step, a borazine saturated surface was heated to 653 K (Figure 1b). This is a temperature, where ultraviolet photoemission spectroscopy (UPS) shows an almost complete disappearance of the feature associated with the B−N σ bond, thus signaling cracking of the B−N rings, presumably even down to the atomic constituents.[18] The 2D autocorrelation (Figure 1d) contains no traces of the (1 × 2) m.r. reconstruction any more. Instead, the Pt(110) surface seems to be disordered. The rms roughness is slightly increased to 55 pm. Obviously, the chemical activity of the fragment radicals is now attacking the Pt surface, lifting the (1 × 2) reconstruction and causing some disorder.

Next, a borazine layer was annealed to 973 K for 3 min (Figure 2a). This increases the rms roughness markedly to 93 pm. Another conspicuous detail is the occurrence of small patches featuring parallel rows. The distance between the rows is about 460 pm, i.e., about 70 pm larger than the distance between close-packed rows on an ideal (1 × 1) Pt(110) surface. Annealing to 1143 K for 1 min (Figure 2b) causes a reorganization of almost the complete surface into patches of such a parallel row structure. Occasionally, a few rows deviate slightly from the [1−10] direction. Finally, upon further annealing of the borazine adlayer at 1143 K for 4 min (Figure 2c), the characteristic moiré pattern of an h-BN monolayer on Pt(110) appears (for a detailed analysis of h-BN/Pt(110) see Steiner et al.[14] A brief summary is provided in the Supporting Information Figure S2). Simultaneously, desorption causes a substantial loss of material, leaving clean surface areas with unequally distributed Pt rows and several <1−10> steps but

https://doi.org/10.1021/acs.jpcc.3c00206
J. Phys. Chem. C 2023, 127, 11559−11569

partially exhibiting the (1 × 2) m.r. structure of clean Pt(110). The residual coverage of 67 ± 6% was estimated by manually tracing out the h-BN islands and determining their area. The intense electron bombardment required for heating the sample to $T \geq 1143$ K results in a significant stray-electron current. In addition, radiation heating of surrounding structures produces a background pressure rise to some 10^{-8} mbar. Both effects concur in hindering an identification of the desorbing species by mass spectrometry. Substantial amounts of B are dissolved in the Pt bulk after such preparations. In fact, after sputter-cleaning the surface, the dissolved B can be segregated again to the surface by prolonged annealing to ∼1100 K and causes growth of borophene islands. Studies of borazine decomposition on different metallic substrates indicate a complete disintegration into its atomic constituents at high temperature. Hence, we conclude that the desorbing species is predominantly N_2, rather than BN.

Close inspection of the parallel-row patterns appearing on a few spots in Figure 2a (blue profile) and in most areas of Figure 2b (red profile 1) reveal a slight corrugation along the rows, which agrees with the periodicity of the h-BN/Pt(110) moiré pattern in the [1−10] direction. This signals formation of h-BN islands on top of the Pt rows. In some cases, the edges of these speckles are aligned with the directions expected for triangular islands, whereby the baseline—the BN zigzag chains—run parallel to the [1−10] direction, i.e., to the Pt close-packed rows, as indicated by the white triangles in Figure 2b enclosing such nuclei. It seems that left- and right-oriented shapes are present, as expected for nucleation of twinned domains.

Upon prolonged annealing of 10 min at 1143 K, the moiré pattern is markedly improved, and the (1 × n) m.r. reconstruction is detectable below the islands (Figure 3a). The Pt row-to-row distance is reduced to ∼420 pm as in the perfect film. The well-developed moiré pattern allows identifying islands, which are slightly rotated away from the ideal orientation. Close inspection reveals series of kinks in the underlying Pt row structure (see Figure S5 in the Supporting Information). Single kinks are also occasionally observed in perfect h-BN films on Pt(110).[14] The coverage is reduced to about 40% (as opposed to 67% after 3 min annealing, see Figure 2c). Obviously, desorption is slow but non-negligible at 1143 K.

Short flash annealing of a freshly deposited borazine layer to 1193 K complements the annealing series (Figure 3b). Due to the short duration of the heat pulse, less material is lost in desorption. What remains on the surface is apparently completely converted into h-BN as indicated by the moiré pattern. The imperfect quality of the moiré pattern is due to some disorder of the Pt atom rows below the h-BN monolayer. This is particularly obvious in the lower left part of the STM image, where the Pt atom rows appear wavy and often interrupted. Even in regions, where the moiré pattern is rather clearly developed, the Pt surface underneath does not yet exhibit the (1 × n) m.r. structure characteristic of a perfectly equilibrated h-BN monolayer on Pt(110).[14]

Independently from the annealing history, we found in all cases persisting fault lines between merged islands (arrows in Figure 3b and Figures S3−S5 in Supporting Information). The fault lines are characterized by breaks in the moiré periodicity and by interruptions or slight misalignment of the underlying Pt close-packed rows, as explained in the Supporting Information. The persistence of fault lines conforms to the observations of Dong et al.[10] They, too, were unable to avoid or anneal fault lines between h-BN nuclei coalescing on Rh(111).

In the annealing experiments of preadsorbed borazine, we find in the STM images first h-BN islands only after short annealing to at least ∼970 K. Complementing the STM studies, UV photoemission spectroscopy (PES) yields some information about the reactions in the borazine adlayer at lower temperatures preceding the h-BN formation. Studies of borazine adsorption on various substrates agree that borazine is decomposed into atomic moieties already at moderate temperatures.[18,25,26] Obviously, the atomic building blocks have to reassociate again to form the h-BN islands at higher temperatures. Interestingly, atomic nitrogen adsorbed on Pt(110) (Rh(111)) has been reported to desorb below 600 K (700 K).[27] In contrast, neither in our investigation of borazine decomposition[18] nor in the study of Frenken and co-workers[10] was a notable loss of nitrogen observed when the temperature was ramped up to ∼1000 K. There are only two explanations for this result: either borazine decomposes only into BN dimers and not into atomic moieties or N recombination is hindered, because recombination sites are blocked. Note that a recombination-site blocking for H−H recombination, in this case definitively of short-bridge sites, is also signaled by the shape of the hydrogen temperature-programmed desorption spectrum of borazine/Pt(110).[18] PES indicates B−N bond formation in the temperature interval between 653 and 973 K. Upon annealing to $T \geq 673$ K the work function drops by almost 0.5 eV,[18] and a significant change occurs in the binding energy region between 3 and 12 eV. A new peak appears at ∼4.6 eV and a new shoulder at about 11 eV (see Figure S6 in Supporting Information). These binding energies correspond approximately to the top of the σ bands at $\bar{\Gamma}$ and the bottom of the σ bands at $\bar{K}$ in the h-BN monolayer on Pt(110).[28] Since in this temperature range the surface is disordered, $k_{\parallel}$ is not a good quantum number, and the UPS spectrum reflects essentially the density of states. Accordingly, we take these features as fingerprint for the incipient formation of extended B−N bonds.

Exposure of the Pt(110) surface to borazine at 100 K and subsequent annealing to 970 K results in a rough surface. However, deviation from a mean surface plane is essentially limited to one or two step heights (138 and 276 pm, respectively; see Figure S1 in the Supporting Information). This is the characteristic property of a so-called disordered flat surface expected above the preroughening temperature but below the roughening phase transition.[29] In the present case, it develops as a consequence of h-BN island formation: since below h-BN the (1 × 2) m.r. Pt(110) surface reconstruction is lifted, the Pt atom rows underneath the film condense into (1 × 1) islands, exposing the second Pt layer, which however remains in the (1 × 1) configuration, if it is covered by h-BN as well. Thus, h-BN deposition on an ideally smooth (1 × 2) m.r. reconstructed surface would result in approximately 50% island area stochastically distributed over the surface, if long-range transport is excluded.[30]

3.2. Protocol 2: h-BN Monolayer Preparation at 970 K and Subsequent Annealing. For an h-BN film formed upon borazine vapor exposure at 970 K, the evolution of the roughness upon successively higher annealing steps was followed by measurements of root-mean-square (rms) surface roughness and that of the h-BN quality by the development of low-energy-electron-diffraction (LEED) spots (for technical

https://doi.org/10.1021/acs.jpcc.3c00206
J. Phys. Chem. C 2023, 127, 11559−11569

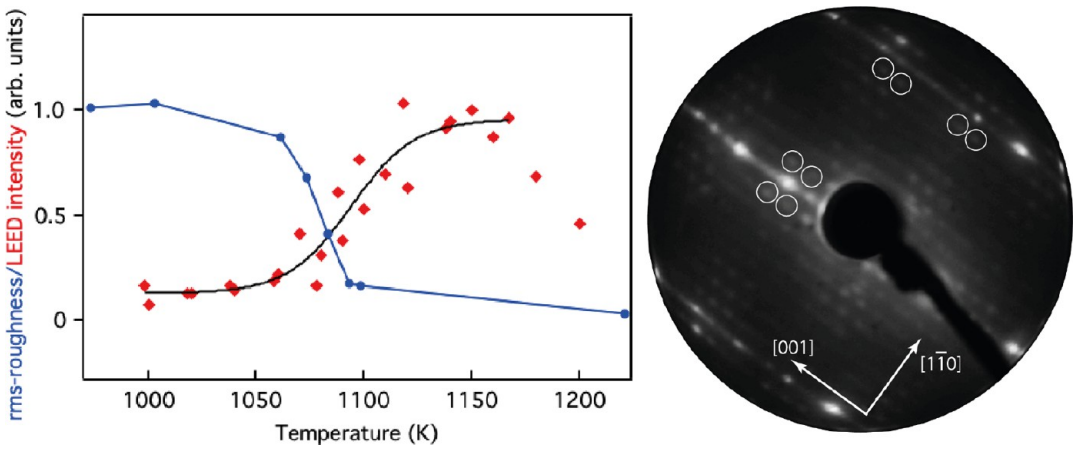

Figure 4. rms roughness (blue) and relative LEED intensity $(I_T - I_{1000K})/(I_{1120K} - I_{1000K})$ (red diamonds) of a moiré superstructure spot as a function of successively higher annealing temperature for an h-BN layer deposited by borazine exposure at 970 K. The black curve is a guide to the eye through the LEED results. The decrease above ∼1160 K is due to desorption. A LEED image recorded after annealing to 1200 K at E_p = 62 eV is shown in the right panel. The spots used for the intensity measurements are marked by circles. A baseline was subtracted from the rms roughness data, and the resulting curve was normalized to 1 for easier comparison with the LEED data.

details see Supporting Information). The results are shown in Figure 4.

The decrease of the rms roughness can be rationalized in the following way: With a perfect h-BN film deposited at 1120 K, we find much larger terraces than on the pristine surface.[14] In the present preparation, the fragmented film evolves upon successively higher annealing into larger ordered domains, which each are associated with a flat Pt terrace underneath. Since at T > 1100 K the clean surface is above the roughening temperature, there exists neither a static step structure nor can one define separate terraces.[31] Underneath a growing h-BN island, however, Pt atoms attach to every second BN zigzag row. These h-BN/Pt double layers suppress the formation of steps underneath. In the spirit of the Laplacian roughening model,[32] the stiffness of the h-BN film adds an energy term $\sum_{\vec{r}} |\Delta h(\vec{r})|^2$ to the surface free energy,[33] with $\vec{r}$ designating lattice sites and h being an integer height coordinate relative to a reference plane. In simple words, warping of the h-BN film is energetically unfavorable. Therefore, upon cooling, the h-BN covered surface areas tend to form large terraces and local deviations from the ideal (110) surface orientation, resulting in multiple step heights rather than distributed single steps (step bunching, see Figure S7 in Supporting Information). Note, however, that the saturation of the LEED intensity shown in Figure 4 does not correspond to reaching the maximum terrace size at the given nucleation density, since at 1150 K, terrace growth is already competing with desorption.

It is noteworthy that the reduction of the rms roughness and the intensity increase of the moiré LEED spot both occur around 1080 K, which is the roughening temperature of the pristine Pt(110) surface[34] as determined by X-ray diffraction. The precise process underlying the corresponding phase transition is not quite clear,[31,35] but it is obviously associated with an essential instability of the Pt(110) surface. This instability allows the attachment of top-layer Pt atoms to the growing h-BN film without requiring long-range transport.

The intensity increase of the moiré superstructure LEED spot continues toward distinctly higher temperatures than the decrease of the surface roughness caused by terrace growth. This indicates an ordering process, which is different from the h-BN growth. The observations reported for the preparation according to protocol 1 reveal that this ordering process is associated with an ordering of the Pt rows underneath the h-BN film. For small h-BN nuclei having a width of only a few Pt rows, the Pt rows are strongly bonded to the BN zigzag rows and therefore incommensurate with the Pt substrate. This is a metastable state, which becomes unstable as the misfit energy grows with the h-BN island size. Once the islands reach sizes of at least one moiré unit cell and the temperature is high enough, the Pt rows relax into the $(1 \times n)$ m.r. configuration with n = 5 or 6 as in the perfect film and thereby reduce the misfit energy.

Figure 5 shows a series of STM images providing a real-space view of the changes occurring at increasing annealing temperatures. The expansion of the terraces is clearly visible as well as the relaxation into the $(1 \times n)$ m.r. structure occurring underneath the larger h-BN domains. At temperatures above ∼1080 K, we also note an onset of desorption and, by inference, of surface diffusion, which on the one hand leads to a slight reduction of the h-BN coverage but on the other hand allows further terrace growth and increase of the remaining islands. We conclude that at these temperatures, material from the edges of h-BN islands is transported both into the gas phase (desorption) and across the surface (surface diffusion), giving rise to Ostwald ripening. In the present case of h-BN island coarsening on Pt(110), Smoluchowski ripening is of minor relevance for reasons detailed in the Supporting Information (p. S10).

3.3. Protocol 3: Exposure to Borazine at T > 1120 K.

In this protocol, extended single-domain growth is observed as reported in ref 14. Step bunching occurs, which leads to the formation of terraces with sizes exceeding 100 × 400 nm^2, i.e., much larger than on the pristine surface. This, however, is not the limit of h-BN domain sizes, since h-BN grows carpet-like also over step edges (see ref 14 for details). Pt rows underneath the h-BN layer arrange into a long-range ordered (1×5) respectively (1×6) m.r. interface (see Figure S2 in the Supporting Information). If the pressure of exposure is reduced below a certain limit, a peculiar result is obtained: some terraces are fully covered by h-BN, and others are completely empty. Examples are shown in the Supporting Information (Figure S8). Occasionally, we found islands fully spanning the terrace width in [001] direction, i.e., from step to

https://doi.org/10.1021/acs.jpcc.3c00206
J. Phys. Chem. C 2023, 127, 11559−11569

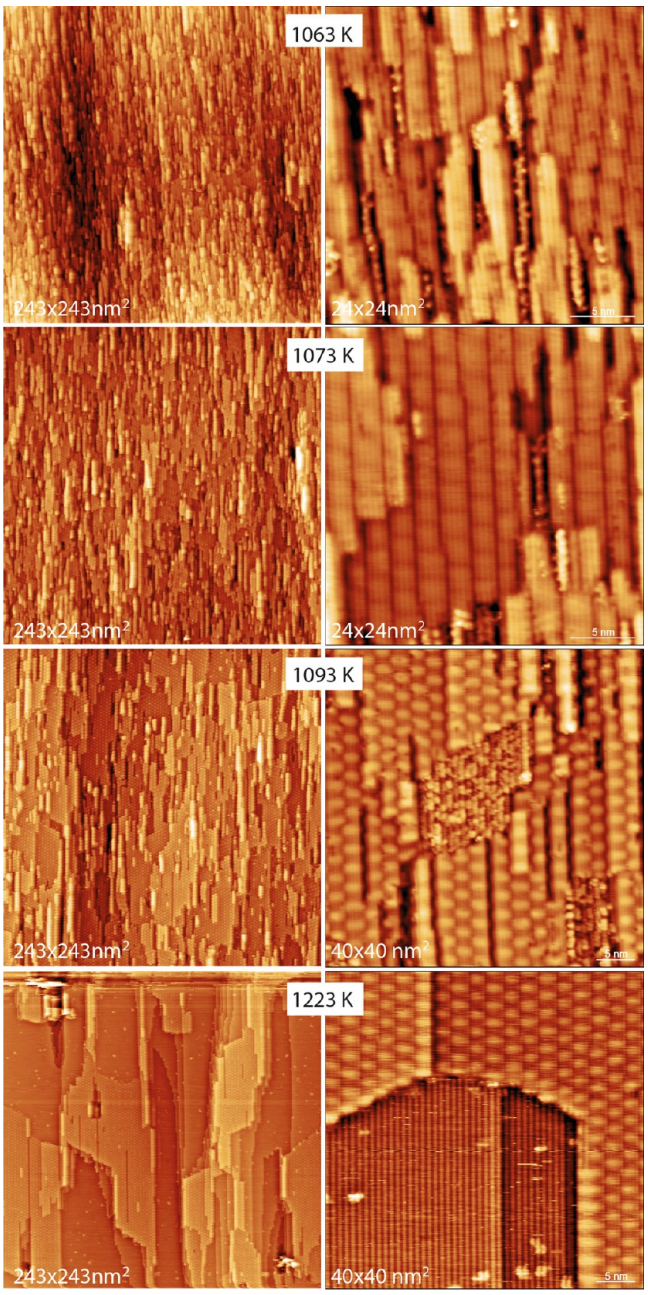

Figure 5. Evolution of an h-BN film deposited at 970 K and successively annealed to the temperatures indicated in the figure (t_{anneal} = 1 min). The rms roughness shown in Figure 5 was determined from such 243 × 243 nm^2 images.

step across the Pt rows but terminating on a terrace with edges of varying orientation in [1−10] direction. As a rule, these edges followed the boundaries of moiré unit cells, which parallels the observations of Dong[10] for h-BN/Rh(111). We were not able to observe triangular h-BN nuclei on a terrace, as it is the case on other metal surfaces such as Cu(111) or Ir(111).

3.4. Theory. To further investigate the increased Pt row-to-row distance of up to 460 pm (compared to a B−N zigzag row distance of 433 pm in the free-standing film), we performed DFT calculations with a moderately reduced BN density (Figure 6) to mimic the interaction of the Pt substrate with the incomplete BN film observed with protocol 1. Indeed, the

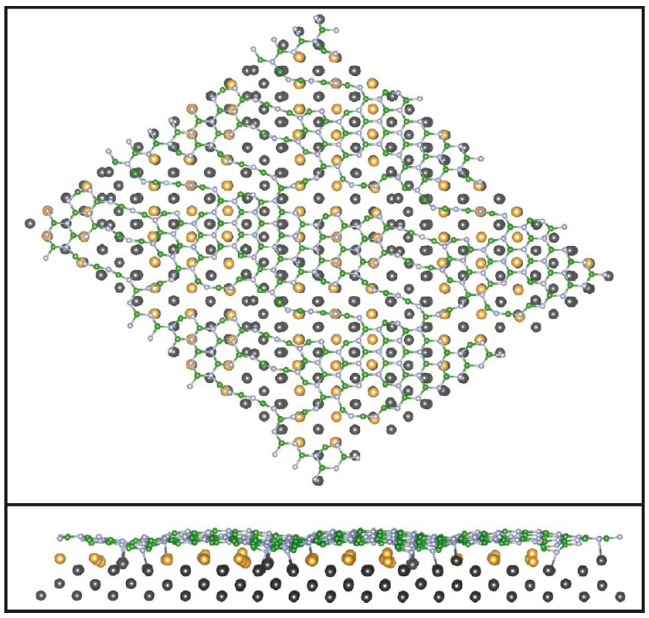

Figure 6. Geometry of a relaxed h-BN film originally stretched along the [1−10] direction in such a way that the bond length in the BN zig-zags along this direction amounted to 172 pm. After relaxation, such a film decays into more isotropic h-BN islands with B−N bond distances between 143 and 148 pm as in the perfect film (see Figure S2 of the Supporting Information). The islands are connected by B−N chains with shorter bond length. The topmost Pt atoms are shown in yellow. Note the strong perturbation of the top Pt layers, which makes it difficult to discriminate between the first and second layers. This indicates a stronger Pt/h-BN interaction for the islands as compared to the perfect film shown in Figure S2.

calculations confirm that the stress in the BN film prevents an extensive stretching and leads to local islands connected by BN chains as shown in Figure 6.

However, the distances between the zigzag rows of the islands are in fact larger than in the free-standing film and amount to about 445 pm. Depending on their position relative to the BN mesh, the Pt atoms underneath display a strong interaction with the h-BN film. In the relaxed configuration, we find Pt distances across the row direction varying from 389 up to 420 pm. In summary, the calculation confirms a significant interaction between the topmost Pt atoms and the h-BN islands, moving even several Pt atoms of the subsurface layer to the surface. The large Pt row-to-row distances observed below the h-BN nuclei in experiment are not reproduced in the relaxed DFT structure shown in Figure 6. We argue that they belong to a metastable configuration.

4. DISCUSSION

There is a fundamental difference between h-BN growth from high-temperature exposure to borazine on the one hand and from preadsorbed borazine and subsequent annealing on the other hand. In the former case, extended single-domain films can be obtained at $T \gtrsim 1120$ K. In the latter case, only h-BN islands with different orientations on a strongly disordered surface are obtained. Underneath the small islands, the Pt row-to-row distance amounts to ∼460 pm (Figure 2b). In the following, we call these structures "460 pm islands" for brevity. Upon annealing to 1143 K, the islands grow on a time scale of several minutes and transform into islands featuring a moiré pattern ("moiré islands"), sometimes with the typical relaxed

https://doi.org/10.1021/acs.jpcc.3c00206
J. Phys. Chem. C 2023, 127, 11559−11569

$(1 \times n)$ m.r. Pt row structure underneath but sometimes also with deviating angular orientation of both the h-BN and the underlying Pt rows (Figures 2c, 3a, and S5). Upon coalescence, fault lines form, which survive various annealing procedures and persist up to the desorption temperature of h-BN. A continuous, single-domain layer cannot be achieved in this way. Obviously, self-collimated growth of single-domain h-BN via electrostatically driven grain reorientation as proposed by Lee et al.[13] for h-BN/Au cannot be the mechanism enabling single-domain growth on Pt(110) and most other metallic templates. Why, then, is high-temperature exposure (protocol 3) able to yield single-domain growth on Pt(110)?

In all annealing experiments described above, the majority of nuclei exhibited zigzag edges parallel to the close-packed row direction of the pristine surface. If nuclei were preferentially formed with zigzag edges along <112> steps, as proposed by Yakobson and co-workers,[15] one should observe a misalignment of ∼5°. It is possible that the small misaligned flakes observed on some spots are due to this effect, but obviously, this is not the origin of most nuclei, which grow into larger single-domain areas. Thus, the mechanism assumed to be responsible for h-BN single-crystal growth on vicinal Cu(110)[15,17] is not operative on Pt(110). Similarly, asymmetric nucleation on steps as proposed for Cu(111) by Chen et al.[16] would not work on Pt(110) with its symmetric step structure.

Following the arguments of Dong et al.,[10] the single-domain growth in protocol 3 could be due to a dramatically reduced nucleation probability, allowing one isolated nucleus to grow into a large single-crystalline domain. In classical nucleation theory, the nucleation density depends on Φ/D, where Φ is the flux and D the temperature dependent surface diffusion coefficient. In Protocols 1 and 2, nucleation starts at temperatures around 970 K, while in protocol 3, nucleation takes place at $T \approx 1120$ K, where the diffusion coefficient is larger and thus tends to reduce the nucleation density. However, in protocol 3, an exposition of 20 s at a background pressure of 5×10^{-8} mbar at 1120 K is sufficient to grow a complete, continuous film; hence, nucleation obviously takes place within seconds. In contrast, the conversion of small "460 pm islands" into larger "moiré islands", which relates to the diffusion coefficient, requires several minutes even at 1143 K. This large difference in time scales is in conflict with a nucleation density low enough for single domains to grow well-beyond 400 nm.

Furthermore, in protocol 3, the h-BN film is always perfectly oriented with the B−N zig-zags in [1−10] direction, in contrast to the islands seen in Figures 2c, 3a, and S5. Since a rotation or reconfiguration of islands at 1120 K is a matter of minutes at least (note the persistence of an oblique h-BN patch in Figure 2c after 1 min at 1143 K), the nucleation mechanism in protocol 3 seems to be qualitatively different, because it never results in an oblique structure. To explain the results, we propose a two-step nucleation mechanism in protocol 3: the first step is the formation of "460 pm islands" as observed in protocol 1. The covalent bonding of on-top N to Pt[14,28] leads to an effective attraction of the B−N zigzag rows and the Pt atom rows in such a way that every second zigzag row bonds to a (perturbed) Pt row. Accordingly, the Pt row-to-row distance is significantly larger than on a (1×1) bulk terminated Pt surface. At this stage, the h-BN islands can be considered to consist of an h-BN/Pt double layer, which is incommensurate with the Pt bulk underneath. Due to the misfit energy, these islands are not very stable. In protocol 3, borazine exposure is associated with a dramatic rise of H_2 background pressure owing to borazine decomposition. Hydrogen is an etchant effectively removing h-BN.[36] Thus, the small, unstable islands are rapidly eroded by etching. If, however, a nucleus exceeds by chance a size of the order of a few moiré supercells and is well-oriented, the Pt rows relax in the $(1 \times n)$ m.r. configuration characteristic for the perfect film. This releases a large part of the misfit energy and stabilizes the h-BN island, which is now less susceptible to etching and grows rapidly in the high borazine flux. Thus, the nucleation proceeds in two steps: First, formation of incommensurate h-BN/Pt double-layer nuclei and then relaxation of the Pt rows into the final configuration shown in ref 14. Note that the latter step requires temperatures above 1100 K and a time scale of several minutes even at 1140 K. Thus, a free energy barrier separates the "460 pm islands" from the relaxed state. Such a nonclassical, two-step nucleation can yield an extremely low nucleation density with the simultaneous requirement of high supersaturation without which the second step cannot be completed but which would oppose a low nucleation density in classical nucleation.

In this model, the free-enthalpy barrier between the metastable h-BN/Pt nuclei (i.e., the "460 pm islands") and the final stable configuration ("moiré islands") is associated with the reorganization of the Pt rows. This is supported by the observation of disordered, meandering, and bifurcate Pt rows as they appear in Figure 3b.

In classical nucleation theory, fluctuations lead to the formation and the decay of nuclei. Below a critical size, they have a higher free enthalpy than the state from which they emerge, because the expense in surface free enthalpy ΔG_{surf} ($\propto n^{2/3}$ in 3D or $\propto n^{1/2}$ in 2D, n being the number of atoms in the nucleus) exceeds the gain in volume (respectively area) free enthalpy $\Delta G_{vol}(\propto n)$. Once a nucleus grows large enough, the volume free enthalpy dominates, and further growth of the nucleus is downhill in G. In many cases, however, particularly in biological systems, nucleation is more complicated.[37−40] The first step toward a crystalline phase, for instance, is frequently the formation of a precursor, i.e., an amorphous dense aggregate, which upon reaching a critical size has to overcome a second free-enthalpy barrier to rearrange into a crystalline phase. The present case represents an analogous nonclassical, two-step nucleation mechanism, with the "460 pm islands" representing the precursor, which after reaching a critical size rearranges into the relaxed $(1 \times n)$ m.r. structure. A sketch of the free-enthalpy landscape is provided in Figure 7. Of course, the relative height of the free-enthalpy barriers depends on the temperature.

For nonclassical, two-step nucleation, the generally used (slightly simplified) expression for the nucleation rate J is[38,39]

$$J = \frac{U_2 \exp\left(-\frac{E_2}{k_B T}\right)}{1 + \frac{U_1}{U_0}\exp\left(\frac{\Delta G}{k_B T}\right)} = \frac{U_2 \exp\left(-\frac{E_2}{k_B T}\right)}{1 + \frac{U_1}{U_0}\exp\left(\frac{\Delta H}{k_B T} - \frac{\Delta S}{k_B}\right)}$$

with U_i being a pre-exponential factor for process i, containing the concentration of the respective phase and the Zeldovich factor. Process 0 is the formation of the precursor islands, process 1 the reverse process, i.e., decay of these islands, which in the present case is predominantly caused by hydrogen etching, and process 2 the forward reaction to the relaxed h-BN film. The formula is obtained under the assumption $U_2 \ll U_0$. E_2 is the free-enthalpy barrier for the relaxed h-BN

https://doi.org/10.1021/acs.jpcc.3c00206
J. Phys. Chem. C 2023, 127, 11559−11569

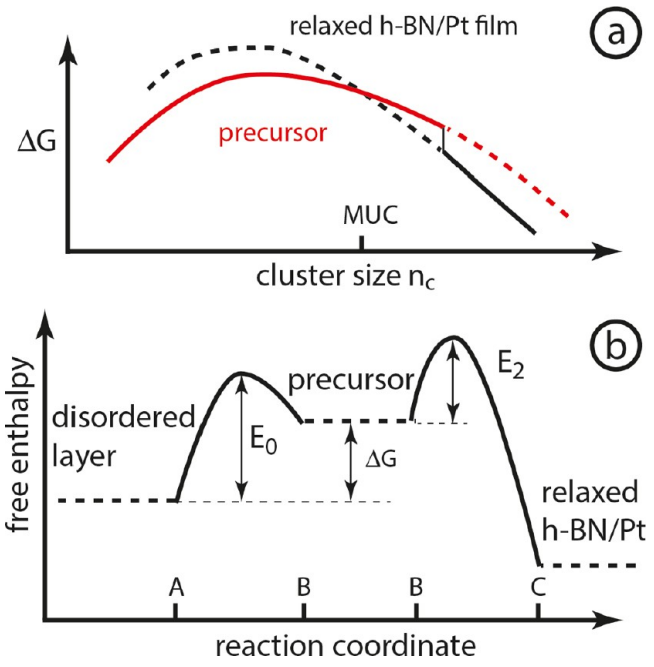

Figure 7. Schematic of the free-enthalpy landscape in the two-step nucleation process. (a) Schematic free-enthalpy difference (at high temperature) between the disordered layer and the BN clusters as a function of island size (MUC = moiré unit cell); red curve: precursor; black curve: islands with a $(1 \times n)$ m.r. h-BN/Pt(110) structure (relaxed h-BN/Pt film). The curve crossing is due to the increase of precursor−substrate misfit energy with island size. Solid line: Trajectory in the two-step nucleation process. Precursor islands grow beyond the thermodynamic equilibrium point, because the precursor is kinetically arrested by the free-enthalpy barrier E_2. (b) Schematic free-enthalpy barriers in the two-step nucleation process. E_0 is the free-enthalpy barrier between the disordered layer and the precursor, E_2 the free-enthalpy barrier for conversion of the precursor into relaxed h-BN/Pt. *A*, *B*, and *C* are points along the reaction coordinate. The change in reaction coordinate from *A* to *B* relates essentially to the formation and growth of h-BN nuclei with Pt rows underneath every second zigzag chain; from B to C, the Pt rows rearrange into the $(1 \times n)$ m.r. pattern releasing the misfit energy to a large extent.

formation. The numerator is the same expression as in classical nucleation theory. ΔG is the free-enthalpy difference between the disordered adlayer and the precursor islands. Note that the free-enthalpy barrier E_1 between the disordered and the precursor configuration does not appear in the expression for the nucleation rate. Due to the loss of entropy upon forming the ordered precursor islands, ΔG increases with temperature. In contrast, the entropy change for the second step (relaxation of Pt atom rows) is small, and therefore, E_2 can be considered as a temperature independent, almost purely energetic barrier. The above expression allows for a nonmonotonic dependence of the nucleation rate on temperature, i.e., an increase up to a certain temperature and a subsequent steep drop in nucleation rate as the temperature is further increased (see Figure S9 in the Supporting Information). This is in qualitative agreement with the observation of an h-BN film without long-range order at growth temperatures below 1100 K[19] and extended single-crystal growth above 1120 K.[14]

The two-step model also provides a rationale for the virtual absence of isolated h-BN islands on terraces in the high-temperature exposure protocol at short exposure times or low pressures. Such conditions suppress the number of precursor islands reaching the critical size required for jumping over the free-enthalpy barrier E_2. The latter process is only possible if the gas phase pressure corresponds to a massive supersaturation. Accordingly, once an island crosses the barrier, the island grows rapidly, quickly acquiring a considerable size. Due to the comparatively strong interaction of Pt rows with the BN zigzag rows, the edge energies of such islands are different from those of unsupported h-BN flakes; hence, no triangular shapes are observed in this preparation protocol.

We conclude the discussion with a few remarks on h-BN nucleation on Cu. Cu has been suggested as one of the best-suited templates for h-BN growth. Kidambi et al.[41] observed that oxygen pre- or cofeeding during borazine deposition on Cu reduced the h-BN nucleation density and improved the film quality as a consequence of the oxygen etching effect. Here, the hydrogen etching[36] assists in suppressing the nucleation density. Large-scale, single-domain growth has been achieved on both Cu(111)[16] and vicinal Cu(110).[17] In contrast to the present experiments, multiple nucleation with a uniform orientation was observed. Accordingly, the single-domain growth was attributed to seamless merging of identically oriented nuclei. This was rationalized in terms of h-BN nucleation at steps with a favorable step-h-BN edge binding energy.[15,16,42] However, whether step-induced alignment on Cu is a sufficient explanation for the observed single-crystal films is not entirely clear. h-BN film growth on Cu is carried out at temperatures where the Cu vapor pressure is already non-negligible. Surface atom mobility is very high at these temperatures, and it is not clear if nucleation models based on a defined step geometry yield a realistic description of the process. Wu et al.[12] report that preannealing in Ar flux and a certain H_2 flux are crucial for optimum alignment. Herrmann, too, reported that hydrogen seemed essential for a more uniform alignment of nuclei on Cu(110).[43] In any case, the detailed mechanism of nucleation and growth of large single-domain h-BN on Cu deserves to be examined again in more detail.

5. CONCLUSIONS

Nucleation of h-BN on Pt(110) occurs in a nonclassical two-step process. The first nucleation step is the nucleation of an incommensurate dynamic h-BN/Pt double layer on the Pt substrate. The second step occurs for h-BN islands reaching a critical size of the order of a moiré unit cell. It consists of a relaxation of the Pt top atoms into a $(1 \times n)$ m.r. structure, which is a compromise between the h-BN and the Pt bulk periodicity in the spirit of the Frenkel-Kontorova model.[44] During high-temperature exposure ($T > 1100$ K) to borazine, the metastable nuclei forming in the first step are subject to (slow) desorption and to hydrogen etching. These processes hinder their growth to a size for the second step to occur. In order to surmount the second barrier at all, a high supersaturation is required, contrasting the low-flux condition for low nucleation density in classical nucleation.[10] As a consequence, the density of stable nuclei is extremely low, but once such a nucleus has formed, it grows explosively into a large single-domain island.

When overgrown by h-BN, Pt surface areas are converted from the (1×2) m.r. configuration into a $(1 \times n)$ m.r. configuration (n alternating between 5 and 6). If growth proceeds at $T > T_{rough}$, the pristine surface is disordered, but the growing h-BN film serves as a kind of inverted template to

https://doi.org/10.1021/acs.jpcc.3c00206
J. Phys. Chem. C 2023, 127, 11559−11569

which, upon cooling, Pt atoms attach along BN zigzag rows. The resulting h-BN/Pt double layer in turn favors formation of large terraces as T falls below T_{rough} and therefore induces step bunching. Accordingly, the surface morphology after deposition of a uniform h-BN film is dominated by large terraces and double steps.

The observation of large-scale, single-domain growth of h-BN on Pt(110) is thus neither attributable to self-collimated h-BN growth as on liquid Au nor to nucleation at <112> steps, as proposed by Yakobson and co-workers.[15] Rather it is due to a combination of Ostwald ripening of metastable and extremely low nucleation density of stable nuclei. Low nucleation density being a key for single-domain h-BN growth on Rh(111) was also postulated by the Frenken group.[10] A profound difference between Pt(110) and Rh(111), however, stems from the nucleation mechanism, which on all rigid substrates, such as Rh(111), Ir(111), Ru(0001), etc., is expected to follow the classical paradigm of one-step nucleation. Our observation of nonclassical nucleation conforms to the conjecture of Fei et al.,[45] who assume a widespread occurrence of indirect nucleation pathways also in 2D and 3D solid crystallization.

Two-step nucleation of 2D films is an important concept, because it contains additional degrees of freedom for steering the nucleation density. In the present study, for instance, we demonstrated that despite high supersaturation the nucleation density can be suppressed by varying ΔG between parent phase and precursor through choice of appropriate temperatures and independently by chemically reducing the precursor stability through H etching. In contrast, a low nucleation rate in classical nucleation requires low flux and results therefore inevitably in a low growth rate.

■ ASSOCIATED CONTENT

Supporting Information

The Supporting Information is available free of charge at https://pubs.acs.org/doi/10.1021/acs.jpcc.3c00206.

> Surface morphology after borazine preadsorption and subsequent annealing to 970 K (Figure S1); determination of rms roughness and LEED intensity measurements; geometry of a perfect h-BN/Pt(110)-(1 × 5) m.r. film (Figure S2); fault line at the boundary of two perfectly oriented h-BN islands (Figure S3); model of the fault line from Figure S3 (Figure S4); boundary between two misaligned h-BN islands (Figure S5); He I UV photoemission difference spectra recorded after different annealing steps of preadsorbed borazine (Figure S6); characteristic step morphology after preparation of extended single-domain h-BN films (Figure S7); examples of fully h-BN covered and empty (1 × 2) m.r. terraces obtained at insufficient supersaturation for complete coverage (Figure S8); model calculation of relative nucleation rates in a nonclassical nucleation process (Figure S9); Ostwald ripening versus Smoluchowski ripening (PDF)

■ AUTHOR INFORMATION

Corresponding Authors

Dominik Steiner − *Institute of Physical Chemistry, University of Innsbruck, 6020 Innsbruck, Austria*; Email: dominik.steiner@uibk.ac.at

Erminald Bertel − *Institute of Physical Chemistry, University of Innsbruck, 6020 Innsbruck, Austria*; orcid.org/0000-0002-9006-8222; Email: erminald.bertel@uibk.ac.at

Authors

Marco Thaler − *Institute of Physical Chemistry, University of Innsbruck, 6020 Innsbruck, Austria*

Thomas Mairegger − *Institute of Physical Chemistry, University of Innsbruck, 6020 Innsbruck, Austria*; orcid.org/0000-0001-9073-622X

Florian Mittendorfer − *Institute of Applied Physics and Center for Computational Materials Science, Vienna University of Technology, 1040 Vienna, Austria*; orcid.org/0000-0002-5073-9191

Complete contact information is available at: https://pubs.acs.org/10.1021/acs.jpcc.3c00206

Notes

The authors declare no competing financial interest.

■ ACKNOWLEDGMENTS

D.S. and M.T. thank the University of Innsbruck for financial support. F.M. gratefully acknowledges the Vienna Scientific Cluster (VSC) for providing computing time for the DFT calculations.

■ REFERENCES

(1) Yankowitz, M.; Xue, J.; LeRoy, B. J. Graphene on hexagonal boron nitride. *J. Phys.: Condens. Matter* **2014**, *26*, 303201.

(2) Sajid, A.; Ford, M. J.; Reimers, J. R. Single-photon emitters in hexagonal boron nitride: a review of progress. *Rep. Prog. Phys.* **2020**, *83*, 044501.

(3) Lee, I.-H.; He, M.; Zhang, X.; Luo, Y.; Liu, S.; Edgar, J. H.; Wang, K.; Avouris, P.; Low, T.; Caldwell, J. D.; et al. Image polaritons in boron nitride for extreme polariton confinement with low losses. *Nat. Commun.* **2020**, *11*, 3649.

(4) Dai, S.; Fang, W.; Rivera, N.; Stehle, Y.; Jiang, B.-Y.; Shen, J.; Tay, R. Y.; Ciccarino, C. J.; Ma, Q.; Rodan-Legrain, D.; et al. Phonon polaritons in monolayers of hexagonal boron nitride. *Adv. Mater.* **2019**, *31*, 1806603.

(5) Dong, J.; Gao, L.; Fu, Q. Hexagonal boron nitride meeting metal: A new opportunity and territory in heterogeneous catalysis. *J. Phys. Chem. Lett.* **2021**, *12*, 9608−9619.

(6) Yoon, S. I.; Ma, K. Y.; Kim, T.-Y.; Shin, H. S. Proton conductivity of a hexagonal boron nitride membrane and its energy applications. *J. Mater. Chem. A* **2020**, *8*, 2898−2912.

(7) Mandelli, D.; Leven, I.; Hod, O.; Urbakh, M. Sliding friction of graphene/hexagonal -boron nitride heterojunctions: a route to robust superlubricity. *Sci. Rep.* **2017**, *7*, 10851.

(8) Naclerio, A. E.; Kidambi, P. R. A review of scalable hexagonal boron nitride (h-BN) synthesis for present and future applications. *Adv. Mater.* **2023**, *35*, 2207374.

(9) Auwärter, W. Hexagonal boron nitride monolayers on metal supports: Versatile templates for atoms, molecules and nanostructures. *Surf. Sci. Rep.* **2019**, *74*, 1−95.

(10) Dong, G.; Fourré, E. B.; Tabak, F. C.; Frenken, J. W. M. How boron nitride forms a regular nanomesh on Rh(111). *Phys. Rev. Lett.* **2010**, *104*, 096102.

(11) Zhao, R.; Zhao, X.; Liu, Z.; Ding, F.; Liu, Z. Controlling the orientations of h-BN during growth on transition metals by chemical vapor deposition. *Nanoscale* **2017**, *9*, 3561−3567.

(12) Wu, Q.; Park, J.-H.; Park, S.; Jung, S. J.; Suh, H.; Park, N.; Wongwiriyapan, W.; Lee, S.; Lee, Y. H.; Song, Y. J. Single crystalline film of hexagonal boron nitride atomic monolayer by controlling nucleation seeds and domains. *Sci. Rep.* **2015**, *5*, 16159.

(13) Lee, J. S.; Choi, S. H.; Yun, S. J.; Kim, Y. I.; Boandoh, S.; Park, J.-H.; Shin, B. G.; Ko, H.; Lee, S. H.; Kim, Y.-M.; et al. Wafer-scale single-crystal hexagonal boron nitride film via self-collimated grain formation. *Science* **2018**, *362*, 817−821.
(14) Steiner, D.; Mittendorfer, F.; Bertel, E. Quasiliquid layer promotes hexagonal boron nitride (h-BN) single-domain growth: h-BN on Pt(110). *ACS Nano* **2019**, *13*, 7083−7090.
(15) Bets, K. V.; Gupta, N.; Yakobson, B. I. How the complementarity at vicinal steps enables growth of 2D monocrystals. *Nano Lett.* **2019**, *19*, 2027−2031.
(16) Chen, T.-A.; Chuu, C.-P.; Tseng, C.-C.; Wen, C.-K.; Wong, H. S. P.; Pan, S.; Li, R.; Chao, T.-A.; Chueh, W.-C.; Zhang, Y.; et al. Wafer-scale single-crystal hexagonal boron nitride monolayers on Cu (111). *Nature* **2020**, *579*, 219−223.
(17) Wang, L.; Xu, X.; Zhang, L.; Qiao, R.; Wu, M.; Wang, Z.; Zhang, S.; Liang, J.; Zhang, Z.; Zhang, Z.; et al. Epitaxial growth of a 100-square-centimetre single-crystal hexagonal boron nitride monolayer on copper. *Nature* **2019**, *570* (7759), 91−95.
(18) Haug, L.; Roth, J. P.; Thaler, M.; Steiner, D.; Menzel, A.; Tosoni, S.; Pacchioni, G.; Bertel, E. Precursor chemistry of h-BN: adsorption, desorption, and decomposition of borazine on Pt(110). *Phys. Chem. Chem. Phys.* **2020**, *22*, 11704−11712.
(19) Achilli, S.; Cavaliere, E.; Nguyen, T. H.; Cattelan, M.; Agnoli, S. Growth and electronic structure of 2D hexagonal nanosheets on a corrugated rectangular substrate. *Nanotechnology* **2018**, *29*, 485201.
(20) Kresse, G.; Furthmüller, J. Efficient iterative schemes for ab initio total-energy calculations using a plane-wave basis set. *Phys. Rev. B* **1996**, *54*, 11169.
(21) Kresse, G.; Hafner, J. Ab initio molecular dynamics for liquid metals. *Phys. Rev. B* **1993**, *47*, 558−561.
(22) Perdew, J. P.; Burke, K.; Ernzerhof, M. Generalized gradient approximation made simple. *Phys. Rev. Lett.* **1996**, *77*, 3865−3868.
(23) Grimme, S.; Antony, J.; Ehrlich, S.; Krieg, H. A consistent and accurate ab initio parametrization of density functional dispersion correction (DFT-D) for the 94 elements H-Pu. *J. Chem. Phys.* **2010**, *132*, 154104.
(24) Nečas, D.; Klapetek, P. Gwyddion: an open-source software for SPM data analysis. *Cent. Eur. J. Phys.* **2012**, *10*, 181−188.
(25) He, J. W.; Goodman, D. W. Interaction of borazine with a Re(0001) surface, studied by LEED, TDS, AES and ELS. *Surf. Sci.* **1990**, *232*, 138−148.
(26) Orlando, F.; Larciprete, R.; Lacovig, P.; Boscarato, I.; Baraldi, A.; Lizzit, S. Epitaxial growth of hexagonal boron nitride on Ir(111). *J. Phys. Chem. C* **2012**, *116*, 157−164.
(27) Berkó, A.; Solymosi, F. Adsorption of nitrogen atoms on Cu(111), Rh(111) and Pt(110) surfaces. *Appl. Surf. Sci.* **1992**, *55*, 193−202.
(28) Thaler, M.; Steiner, D.; Menzel, A.; Mittendorfer, F.; Bertel, E. Single-domain h-BN on Pt(110): Electronic structure, correlation, and bonding. *Phys. Rev. Res.* **2020**, *2*, 043156.
(29) den Nijs, M. Interplay between Surface Roughening, Preroughening, and Reconstruction. *Phase Transitions in Surface Films* **1991**, *2*, 247−267.
(30) Monine, M. I.; Pismen, L. M. Realistic kinetic Monte Carlo study of the surface phase reconstruction. *Phys. Rev. E* **2004**, *69*, 021606.
(31) Koch, R.; Sturmat, M. High-temperature STM of the phase transitions of Au(110) and Pt(110). *Surf. Sci.* **1998**, *402−404*, 861−865.
(32) Nelson, D. R. Laplacian roughening models and two-dimensional melting. *Phys.l Rev. B* **1982**, *26*, 269−283.
(33) Lee, J. H.; Kim, J. M. Single transition of discrete Laplacian roughening model on a square lattice. *J. Stat. Mech.: Theory Exp.* **2022**, *2022*, 023206.
(34) Robinson, I. K.; Vlieg, E.; Kern, K. Non-Ising behavior of the Pt(110) surface phase transition. *Phys. Rev. Lett.* **1989**, *63*, 2578−2581.
(35) Robinson, I. K.; Vlieg, E.; Kern, K. Robinson, Vlieg, and Kern reply. *Phys. Rev. Lett.* **1990**, *65*, 1831−1831.
(36) Yin, J.; Yu, J.; Li, X.; Li, J.; Zhou, J.; Zhang, Z.; Guo, W. Large single-crystal hexagonal boron nitride monolayer domains with controlled morphology and straight merging boundaries. *Small* **2015**, *11*, 4497−4502.
(37) Kashchiev, D.; Vekilov, P. G.; Kolomeisky, A. B. Kinetics of two-step nucleation of crystals. *J. Chem. Phys.* **2005**, *122*, 244706.
(38) Pan, W.; Kolomeisky, A. B.; Vekilov, P. G. Nucleation of ordered solid phases of proteins via a disordered high-density state: Phenomenological approach. *J. Chem. Phys.* **2005**, *122*, 174905.
(39) Vekilov, P. G. Nucleation. *Cryst. Growth Des.* **2010**, *10*, 5007−5019.
(40) De Yoreo, J. J.; Gilbert, P. U. P. A.; Sommerdijk, N. A. J. M.; Penn, R. L.; Whitelam, S.; Joester, D.; Zhang, H.; Rimer, J. D.; Navrotsky, A.; Banfield, J. F.; et al. Crystallization by particle attachment in synthetic, biogenic, and geologic environments. *Science* **2015**, *349*, aaa6760.
(41) Kidambi, P. R.; Blume, R.; Kling, J.; Wagner, J. B.; Baehtz, C.; Weatherup, R. S.; Schloegl, R.; Bayer, B. C.; Hofmann, S. In situ observations during chemical vapor deposition of hexagonal boron nitride on polycrystalline copper. *Chem. Mater.* **2014**, *26*, 6380−6392.
(42) Zhang, L.; Ding, F. The stable interfaces between various edges of hBN and step edges of Cu surface in hBN epitaxial growth: a comprehensive theoretical exploration. *2D Mater.* **2021**, *8*, 034004.
(43) Herrmann, C. *In situ observations of hexagonal boron nitride growth on Cu(110)*, Ph.D. Thesis. Simon Fraser University, Burnaby, 2020.
(44) Bak, P. Commensurate phases, incommensurate phases and the devil's staircase. *Rep. Prog. Phys.* **1982**, *45*, 587.
(45) Fei, L.; Gan, X.; Ng, S. M.; Wang, H.; Xu, M.; Lu, W.; Zhou, Y.; Leung, C. W.; Mak, C.-L.; Wang, L. Observable two-step nucleation mechanism in solid-state formation of tungsten carbide. *ACS Nano* **2019**, *13*, 681−688.

https://doi.org/10.1021/acs.jpcc.3c00206
J. Phys. Chem. C 2023, 127, 11559−11569